

Fully Quantum Approach to Optomechanical Entanglement

Qing Lin,^{1,2} Bing He,^{1,3} R. Ghobadi,⁴ and Christoph Simon¹

¹*Institute for Quantum Science and Technology, University of Calgary, Alberta T2N 1N4, Canada*

²*College of Information Science and Engineering, Huaqiao University, Xiamen 361021, China*

³*Department of Physics, University of Arkansas, Fayetteville, AR 72701, USA*

⁴*Institute of Atomic and Subatomic Physics, TU Wien, Stadionallee 2, 1020 Wien, Austria*

The radiation pressure induced coupling between an optical cavity field and a mechanical oscillator can create entanglement between them. In previous works this entanglement was treated as that of the quantum fluctuations of the cavity and mechanical modes around their classical mean values. Here we provide a fully quantum approach to optomechanical entanglement, which goes beyond the approximation of classical mean motion plus quantum fluctuation, and applies to arbitrary cavity drive. We illustrate the real-time evolution of optomechanical entanglement under drive of arbitrary detuning to show the existence of high, robust and stable entanglement in blue detuned regime, and highlight the quantum noise effects that can cause entanglement sudden death and revival.

PACS numbers: 03.65.Ud, 03.65.Ta, 05.40.Jc, 42.50.Xa

I. INTRODUCTION

The study of optomechanical systems (OMS) has undergone rapid development over the recent years [1–3]. The quantum level of OMS has been reached in experiments [4–9]. Entanglement is a particularly striking quantum feature. The coupling of the cavity field of an OMS to the mechanical oscillator under radiation pressure can lead to their entanglement. This mesoscopic or macroscopic entanglement possesses both fundamental interest and potential applications.

Theoretically an OMS is often approached via the expansion of its fluctuations about the mean values of the cavity and mechanical mode operators, where these mean values are determined by the classical equations of motion. This approximation of replacing a quantum system operator with the sum of a classical value and the accompanying quantum fluctuation has been widely applied to generic nonlinear quantum systems whose Heisenberg-Langevin equations are not analytically solvable [10]. Most previous studies of optomechanical entanglement (see, e.g. [11–19]) concern that of the fluctuations around the steady state solution of the classical Langevin equations under continuous-wave (CW) drive. Some other

works have considered the entanglement under periodic [20–22] or pulsed drive [23]. A common feature of these treatments is that the linearized dynamics about the fluctuations is based on a specific classical mean motion as the background, and the entanglement of the fluctuations can be closely connected to the classical motion of OMS [24]. However, the classical motion of an OMS can be chaotic [25], so it is not always possible to quantify this entanglement of fluctuations [24].

Very recently several quantum features of OMS have been studied in considerable detail. This research includes OMS dynamics under single photon drive [26–30], control and generation of OMS quantum states [31–36], enhancement of OMS nonlinearity for quantum information processing [37–40] and other quantum properties of OMS [41, 42]. These studies consider the quantum states associated with the cavity mode \hat{a} and mechanical mode \hat{b} themselves, as in Fig. 1, instead of those for their fluctuations. Starting from a separable quantum state of the cavity and mechanical mode, the optomechanical coupling can entangle them to an entangled quantum state. The less unexplored entanglement of such fully quantum OMS, which is independent from classical motion, is the theme to be discussed below. Notice that this type of entanglement was also recently discussed in a different approach [43], which works with the numerical simulation based on the approximate Fokker-Planck equation to find the entanglement signature and other properties.

This paper is organized as follows. In Sec. II, we discuss the dynamics about the OMS in strong drive and weak coupling regime. In this regime the quantum states of an OMS keep to be Gaussian. The real-time evolution and quantum noise effect on the entanglement of such Gaussian states are studied with examples in Sec. III. Then we present a rather detailed discussion about the difference between our concerned entanglement and that of the cavity and mechanical fluctuation in Sec. IV. The conclusions from our study are given in the final section.

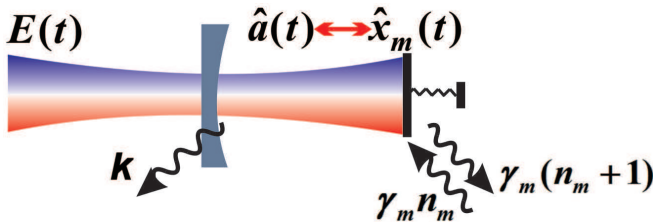


FIG. 1: (color online) Setup for coupling the cavity field $\hat{a}(t)$ with the quantum mechanical oscillator. The cavity field build up by the drive $E(t)$ is entangled with the mechanical oscillator, which is initially in thermal equilibrium with its environment, via their effective coupling described by the Hamiltonian $-\sqrt{2}g\hat{x}_m\hat{a}^\dagger\hat{a}$.

II. DYNAMICS UNDER STRONG DRIVE AND WEAK COUPLING

We consider an OMS driven by a pulsed drive with the central frequency ω_0 and arbitrary frequency distribution $E(\omega - \omega_0)$. Its profile $E(t)e^{i\omega_0 t}$ in time domain is related to $E(\omega - \omega_0)$ by the Fourier transform. The drive reduces to a CW one when $E(t)$ is constant. Without cavity and mechanical damping, one has the unitary evolution operator $U(t, 0) = \exp\{-iH_0 t\} \mathcal{T} \exp\{-i \int_0^t d\tau H_S(\tau)\}$ for the OMS, where $H_0 = \omega_c \hat{a}^\dagger \hat{a} + \omega_m \hat{b}^\dagger \hat{b}$ ($\hbar \equiv 1$) describes the cavity and mechanical oscillation with their frequency ω_c and ω_m , respectively, and

$$H_S(t) = -\sqrt{2}g\{\cos(\omega_m t)\hat{x}_m + \sin(\omega_m t)\hat{p}_m\}\hat{a}^\dagger \hat{a} + iE(t)(\hat{a}^\dagger e^{i\Delta_0 t} - \hat{a}e^{-i\Delta_0 t}) \quad (1)$$

inside the time-ordered exponential is the system Hamiltonian in the interaction picture with respect to H_0 , which is obtained by the transformation $H_S(t) = e^{iH_0 t} H(t) e^{-iH_0 t}$ on the Hamiltonian $H(t) = -g(\hat{b} + \hat{b}^\dagger)\hat{a}^\dagger \hat{a} + iE(t)(\hat{a}^\dagger e^{-i\omega_0 t} - \hat{a}e^{i\omega_0 t})$ of the OMS. In the above equation, g is the optomechanical coupling constant, and $\Delta_0 = \omega_c - \omega_0$ is the detuning of the drive's central frequency from the cavity frequency. The dimensionless mechanical coordinate operator and mechanical momentum operator are defined as $\hat{x}_m = (\hat{b} + \hat{b}^\dagger)/\sqrt{2}$ and $\hat{p}_m = -i(\hat{b} - \hat{b}^\dagger)/\sqrt{2}$, respectively. The cavity (mechanical) damping at the rate κ (γ_m) can be described in terms of a linear coupling between the cavity (mechanical) mode with the stochastic Langevin noise operator $\hat{\xi}_c$ ($\hat{\xi}_m$) of the reservoir [44]:

$$H_D(t) = i(\sqrt{\kappa}\hat{a}^\dagger \hat{\xi}_c(t) + \sqrt{\gamma_m}\hat{b}^\dagger \hat{\xi}_m(t)) + H.c. \quad (2)$$

The associated noises are assumed to be the white ones satisfying $\langle \hat{\xi}_l(t) \hat{\xi}_l^\dagger(\tau) \rangle_R = (n_l + 1)\delta(t - \tau)$ ($l = c, m$) with the respective quanta number n_l in thermal equilibrium. Such approximation is valid for the mechanical reservoir given the quality factor $\omega_m/\gamma_m \gg 1$ [11]. Because the system-reservoir coupling in (2) takes its form in the interaction picture with respect to the total self oscillation Hamiltonian of both system and reservoir, it should be added into the time-ordered exponential $\mathcal{T} \exp\{-i \int_0^t d\tau H_S(\tau)\}$ in the interaction picture to construct the evolution operator $U_S(t, 0) = \mathcal{T} e^{-i \int_0^t d\tau (H_S(\tau) + H_D(\tau))}$ for the combination of the OMS and its associated reservoirs (its momentary action $U_S(t+dt, t)$ gives the exact Langevin equation and master equation of the OMS) [44].

The development of the entanglement between the cavity and mechanical mode is closely connected to the dynamical evolution of these modes. Their evolution under $U_S(t, 0)$ involves three non-commutative processes—cavity drive, optomechanical coupling and dissipation, so it is impossible to solve the system dynamics directly from this joint evolution operator. Our method to reduce the intricacy is factorizing it into numerous ones

corresponding to relatively tractable processes [29]. Here we apply the technique to find a factorization that is suitable to study the dynamically evolving Gaussian states. Our factorization is obtained as

$$U_S(t, 0) = U_E(t, 0)U_{OM}(t, 0)U_K(t, 0)U_D(t, 0),$$

where $U_D(t, 0) = \mathcal{T} \exp\{-i \int_0^t d\tau H_D(\tau)\}$ (see Appendix A for details). The effective Hamiltonian in the first operator $U_E(t, 0) = \mathcal{T} \exp\{-i \int_0^t d\tau \tilde{H}_E(\tau)\}$ for the pure cavity drive process takes the form

$$\tilde{H}_E(\tau) = iE(\tau)e^{i\Delta_0 \tau} \hat{A}^\dagger(t, \tau) + H.c.,$$

with $\hat{A}(t, \tau) = e^{-\frac{\kappa}{2}(t-\tau)}\hat{a} + \hat{n}_c(t, \tau)$ being the sum of the decayed cavity mode operator and the colored cavity noise operator $\hat{n}_c(t, \tau) = \sqrt{\kappa} \int_\tau^t d\tau' e^{-\kappa(\tau'-\tau)/2} \hat{\xi}_c(\tau')$. The third evolution operator is $U_K(t, 0) = \mathcal{T} \exp\{ig \int_0^t d\tau \hat{K}_m(t, \tau) \hat{A}^\dagger \hat{A}(t, \tau)\}$, where $\hat{K}_m(t, \tau) = \cos(\omega_m \tau) \hat{X}_m(t, \tau) + \sin(\omega_m \tau) \hat{P}_m(t, \tau)$ is a linear combination of the mechanical operators $\hat{X}_m(t, \tau) = \hat{B}(t, \tau) + \hat{B}^\dagger(t, \tau)$ and $\hat{P}_m(t, \tau) = -i\hat{B}(t, \tau) + i\hat{B}^\dagger(t, \tau)$ from $\hat{B}(t, \tau) = e^{-\frac{\gamma_m}{2}(t-\tau)}\hat{b} + \hat{n}_m(t, \tau)$ and $\hat{n}_m(t, \tau) = \sqrt{\gamma_m} \int_\tau^t d\tau' e^{-\gamma_m(\tau'-\tau)/2} \hat{\xi}_m(\tau')$. To the first order of the optomechanical coupling constant g , the effective Hamiltonian in the process $U_{OM}(t, 0) = \mathcal{T} \exp\{-i \int_0^t d\tau \tilde{H}_{OM}(\tau)\}$ of optomechanical coupling is

$$\begin{aligned} \tilde{H}_{OM}(\tau) &= g\hat{K}_m(t, \tau)(\hat{A}^\dagger(t, \tau)D(\tau) + \hat{A}(t, \tau)D^*(\tau) \\ &\quad + |D(\tau)|^2), \end{aligned} \quad (3)$$

where

$$\begin{aligned} D(\tau) &= e^{-\frac{\kappa}{2}(t-\tau)} \int_0^\tau dt' E(t') e^{i\Delta_0 t'} e^{-\frac{\kappa}{2}(t-t')} \\ &\quad + \int_0^\tau dt' [\hat{n}_c(t, t'), \hat{n}_c^\dagger(t, \tau)] E(t') e^{i\Delta_0 t'}. \end{aligned} \quad (4)$$

Under the effective Hamiltonian in (3), the OMS evolves according to the following differential equations: which evolves the cavity and mechanical mode in terms of the following differential equations:

$$\begin{aligned} -i \frac{d\hat{a}}{d\tau} &= g e^{-(\kappa+\gamma_m)(t-\tau)/2} D(\tau) (e^{-i\omega_m \tau} \hat{b} + e^{i\omega_m \tau} \hat{b}^\dagger) \\ &\quad + g e^{-\kappa(t-\tau)/2} D(\tau) \cos(\omega_m \tau) (\hat{n}_m(t, \tau) + \hat{n}_m^\dagger(t, \tau)) \\ &\quad + g e^{-\kappa(t-\tau)/2} D(\tau) \sin(\omega_m \tau) (i\hat{n}_m(t, \tau) - i\hat{n}_m^\dagger(t, \tau)), \\ -i \frac{d\hat{b}}{d\tau} &= g e^{-(\kappa+\gamma_m)(t-\tau)/2} e^{i\omega_m \tau} (D^*(\tau) \hat{a} + D(\tau) \hat{a}^\dagger) \\ &\quad + g e^{i\omega_m \tau - \frac{\gamma_m}{2}(t-\tau)} (\hat{n}_c(t, \tau) D^*(\tau) + \hat{n}_c^\dagger(t, \tau) D(\tau)) \\ &\quad + g e^{i\omega_m \tau - \frac{\gamma_m}{2}(t-\tau)} |D(\tau)|^2. \end{aligned} \quad (5)$$

The \hat{a} (\hat{b}) terms on the right side of (5) are due to the beam-splitter (BS) action in the quadratic Hamiltonian (3), and the \hat{a}^\dagger (\hat{b}^\dagger) terms reflect the coexisting squeezing (SQ) action.

Next we start with an initial OMS state $\rho(0)$ in thermal equilibrium with the environment, i.e. $\rho(0)$ is a Gaussian state as the product of a cavity vacuum and a finite temperature mechanical thermal state. This initial state becomes entangled under optomechanical coupling. Its evolution can be studied by successively acting each factor in the factorized form $U_E(t,0)U_{OM}(t,0)U_K(t,0)U_D(t,0)$ of the joint evolution operator $U_S(t,0)$ on the total initial state $\chi(0) = \rho(0)R(0)$, in which $R(0)$ denotes the reservoir state in thermal equilibrium with $\rho(0)$. One has $U_D(t,0)\chi(0)U_D^\dagger(t,0) = \chi(0)$ since, under thermal equilibrium, the system-reservoir coupling in (2) does not change the state $\rho(0)$ (see Appendix B for details), and $U_K(t,0)$ also keeps $\chi(0)$ invariant because $\hat{A}(t,\tau)|0\rangle_C = 0$ for the combined initial vacuum state $|0\rangle_C$ of the cavity and its zero temperature reservoir. Thus the expectation values of system operators $\hat{O}(t)$ reduce to the following trace over system and reservoir degrees of freedom (see Appendix B for details):

$$\langle \hat{O}(t) \rangle = \text{Tr}_{S \otimes R} \{ U_{OM}^\dagger(t,0) U_E^\dagger(t,0) \hat{O} U_E(t,0) U_{OM}(t,0) \times \chi(0) \}. \quad (6)$$

In weak coupling regime where the Hamiltonian of $U_{OM}(t,0)$ takes the form in (3), the evolved OMS is preserved to be in Gaussian state, because the state $\text{Tr}_R \{ U_E(t,0) U_{OM}(t,0) \chi(0) U_{OM}^\dagger(t,0) U_E^\dagger(t,0) \}$ of the evolved OMS is only determined by the quadratic Hamiltonian in $U_{OM}(t,0)$ and the displacement Hamiltonian in $U_E(t,0)$.

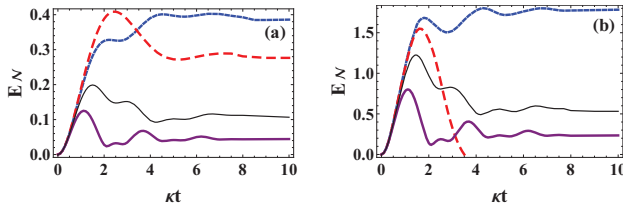


FIG. 2: (color online) Evolution of entanglement for blue detuned CW drives. (a) is obtained with the drive intensity $E/\kappa = 3 \times 10^5$ while (b) is for a drive of $E/\kappa = 2 \times 10^6$. The long dashed (red) curve is for $\Delta_0 = -0.5\omega_m$, the short dashed (blue) curve for $\Delta_0 = -\omega_m$, the thin solid (black) curve for $\Delta_0 = -1.5\omega_m$, and the thick solid (purple) curve for $\Delta_0 = -2\omega_m$. Here $g/\kappa = 10^{-6}$, $\omega_m/\kappa = 2.5$, $\omega_m/\gamma_m = 10^7$, and $T = 0$. The entanglement measure by E_N for these blue detuned drives tends to a stable value with time. The maximum entanglement is reached at the SQ resonant point $\Delta_0 = -\omega_m$. For the stronger drive, the entanglement at the smaller detuning $\Delta_0 = -0.5\omega_m$ dies a sudden death after a finite time period.

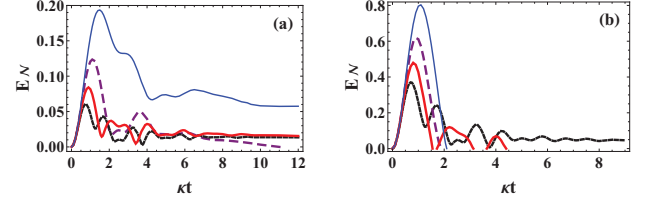


FIG. 3: (color online) Evolution of entanglement for red detuned CW drives. (a) is obtained with the same system parameters as in Fig. 2(a), while (b) is found with the same parameters as in Fig. 2(b). The thin solid (blue) curve is for $\Delta_0 = 0.5\omega_m$, and the long dashed (purple) curve for $\Delta_0 = \omega_m$, the solid (red) curve for $\Delta_0 = 1.5\omega_m$, and the short dashed (black) curve for $\Delta_0 = 2\omega_m$. The entanglement dies earlier for a detuning closer to the BS resonant point $\Delta_0 = \omega_m$ or the stronger drive. Given the stronger drive in (b), the entanglement at $\Delta_0 = 1.5\omega_m$ exhibits sudden death and revival.

III. OMS ENTANGLEMENT

A. Entanglement evolution under CW drive

The entanglement of the evolved Gaussian states can be quantified by the logarithmic negativity E_N [45]. One should consider the correlation matrix (CM) with the elements

$$\hat{V}_{ij}(t) = 1/2 \langle \hat{u}_i \hat{u}_j + \hat{u}_j \hat{u}_i \rangle - \langle \hat{u}_i \rangle \langle \hat{u}_j \rangle,$$

where $\hat{\mathbf{u}} = (\hat{x}_c(t), \hat{p}_c(t), \hat{x}_m(t), \hat{p}_m(t))^T$, for the calculation of E_N (see Appendix C for details). Each entry of the CM can be calculated following (6) with $\hat{O} = \hat{u}_i \hat{u}_j + \hat{u}_j \hat{u}_i$, etc.

We first illustrate the real-time evolution of OMS entanglement under the CW drives of different detuning. The first example we present in Fig. 2 is the entanglement evolution under blue detuned CW drives. The entanglement values measured by E_N become stable with time and, at the SQ resonant point $\Delta_0 = -\omega_m$, the steady entanglement reaches the maximum. Unlike the stationary entanglement between the fluctuations $\delta\hat{a}$ and $\delta\hat{b}$ under a SQ resonant drive, which is upper bounded by $E_N = \ln 2 \approx 0.693$ due to the limitation of classical steady state conditions (see Eq. (7) below) [14], the evolved entanglement between the cavity mode \hat{a} and mechanical mode \hat{b} themselves can be well beyond this limit (see Fig. 2(b)). Compared with the blue detuned regime, the entanglement of the red detuned regime shown in Fig. 3 is lower. This reflects the difference of the BS action from the SQ action in creating the optomechanical entanglement.

B. Quantum noise effect

The exact degree of entanglement is determined by two competitive factors—the direct BS and SQ action

on the initial quantum state $\rho(0)$ of OMS, and the noise drives depending on the drive detuning and intensity. Given a CW drive, the noise drive terms in (5) are magnified by the functions with the modulo $|D(\tau)| = E/\sqrt{0.25\kappa^2 + \Delta_0^2}$, indicating their more significant effect at a small detuning Δ_0 or with a stronger drive intensity E . In what follows, we illustrate the noise effect as a function of time and of different system parameters.

First, the entanglement for some values of detuning in Figs. 2 and 3 will die at a finite time. The phenomenon that entanglement is killed by noise in this way is known as entanglement sudden death (ESD) [46, 47]. The system evolution according to (5) provides a model in which the ESD for the continuous variable states is caused by the colored noises ($\hat{n}_c(t, \tau)$, $\hat{n}_m(t, \tau)$ and their conjugates on the right side of (5)) rather than the white noises in many other examples (see the references in [47]). In this situation the noise effect can be so significant that this type of ESD happens while the optomechanical coupling exists all the time. Interestingly, the entanglement under some drives, e.g. $\Delta_0 = 1.5\omega_m$ in Fig. 3(b), can also revive from time to time during evolution.

Fig. 4 shows the magnitude of the noise correction

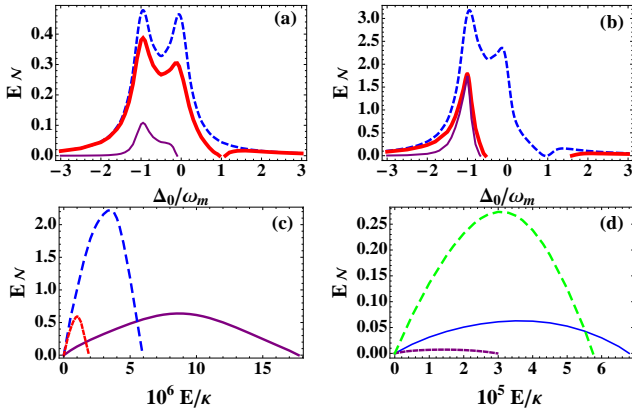


FIG. 4: (color online) (a)-(b): Entanglement versus detuning. (a) is under the same conditions as in Figs. 2(a) and 3(a), and (b) corresponds to the situation in Figs. 2(b) and 3(b). The long dashed (blue) curves show the entanglement obtained at zero temperature without the noise drive terms in (5), while the thick solid (red) curves include the effect of the noise drive terms at zero temperature. In (a) the zero temperature entanglement is eliminated around $\Delta_0 = \omega_m$. The thin solid (purple) curves in (a) and (b) give the exact degree of entanglement at the temperature corresponding to $n_m = 10^4$. (c)-(d): Entanglement versus cavity drive intensity. In (c), the long-dashed curve (blue) stands for $\Delta_0 = -\omega_m$, and the short-dashed curve (red) for $\Delta_0 = -0.5\omega_m$, and the solid (purple) curve for $\Delta_0 = -2\omega_m$. In (d), the long-dashed curve (green) stand for $\Delta_0 = 0$, the short-dashed (purple) curve for $\Delta_0 = \omega_m$, and the solid (blue) curve for $\Delta_0 = 0.5\omega_m$. Except for the thin solid (purple) curves about finite temperature entanglement in (a) and (b), all plots are found for the initial temperature $T = 0$ at the moment $\kappa t = 15$, when the concerned entanglement has stabilized.

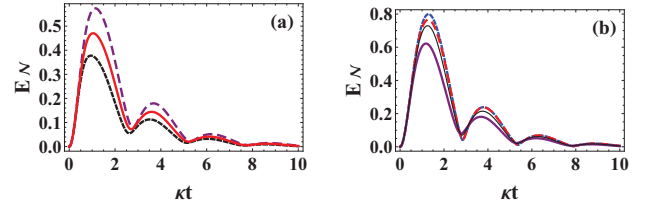


FIG. 5: (color online) Evolution of entanglement under the pulsed drive $E(t) = Ee^{-\Delta\omega^2 t^2}$ with $\Delta\omega = \omega_m$. (a) Red detuned central frequencies. The long dashed (purple) curve is for $\Delta_0 = \omega_m$ of the central frequency, the solid (red) curve for $\Delta_0 = 1.5\omega_m$, and the short dashed (black) curve for $\Delta_0 = 2\omega_m$. (b) Blue detuned and resonant central frequencies. The long dashed (red) curve is for $\Delta_0 = 0$, the short dashed (blue) curve for $\Delta_0 = -\omega_m$, the thin solid (black) curve for $\Delta_0 = -1.5\omega_m$, and the thick solid (purple) curve for $\Delta_0 = -2\omega_m$. The system parameters are $g/\kappa = 10^{-6}$, $E/\kappa = 2 \times 10^6$, $\omega_m/\kappa = 2.5$, $\omega_m/\gamma_m = 10^7$, and $T = 0$. The entanglement measured by E_N goes down at almost same pace for the drives of different central frequency detuning.

to optomechanical entanglement in the system parameter space. Given the same drive intensities, the relations between the entanglement and drive detuning after sufficiently long interaction time are shown in Figs. 4(a)-4(b). With the increase of cavity drive intensity, the entanglement in a more extended detuning range around the BS resonant point $\Delta_0 = \omega_m$ will be eliminated by the quantum noises. The overall tendency of the entanglement change with the drive intensity for various drive detuning values is described in Figs. 4(c)-4(d). The plots in these figures show a competition between the effective coupling $gD(t)$ and the noise drives [see the respective terms in (5)] in affecting the degree of entanglement. The entanglement reaches the maximum at a certain drive intensity E determined by the system parameters, instead of monotonically increasing with E which enhances the effective optomechanical coupling. Despite the existence of the noises, the entanglement in the blue detuned regime can be high. The SQ generated entanglement is also rather robust against temperature; see the comparison in Figs. 4(a) and 4(b).

C. Entanglement evolution under pulsed drive

Finally, in Fig. 5, we provide an example of entanglement evolution for OMS driven by a pulse. Pulsed optomechanics is a newly developed research field [23, 48, 49]. Here we use Gaussian pulses with the width ω_m . Due to the contribution from a spectrum of frequencies, the entanglement for the drives of different central frequency detuning evolves similarly. Another noticeable feature is that, given the same system parameters, the entanglement generated under the pulse could last even longer than that of the CW ones. This can be explained by the contribution from the frequency components out-

side the regime, in which the noise effect quickly destroys the corresponding entanglement. Entanglement under pulsed drive was also discussed in the approach based on classical mean motion background [23]. Like in the CW cases, our results independent of classical background are consequent upon the dynamics involving a significantly different quantum noise effect.

IV. DIFFERENCE FROM ENTANGLEMENT OF FLUCTUATIONS

We are concerned with the regime of strong drive ($E/\kappa \gg 1$) and weak optomechanical coupling ($g/\kappa \ll 1$)

$$\begin{aligned} s_1 &= 2\gamma_m\kappa\{[\kappa^2 + (\omega_m - \Delta)^2][\kappa^2 + (\omega_m + \Delta)^2] + \gamma_m[(\gamma_m + 2\kappa)(\kappa^2 + \Delta^2) + 2\kappa\omega_m^2]\} + \Delta\omega_m G^2(\gamma_m + 2\kappa)^2 > 0, \\ s_2 &= \omega_m(\kappa^2 + \Delta^2) - G^2\Delta > 0, \end{aligned} \quad (7)$$

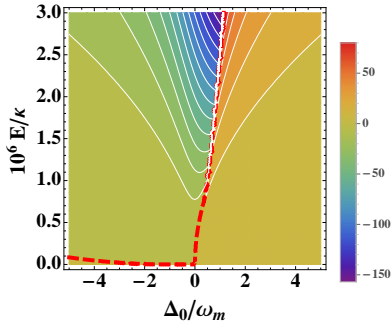


FIG. 6: (color online) The workable regime for the standard fluctuation expansion approach. The scale represents the value of s_1 defined in (7). The second condition $s_2 > 0$ is always satisfied in the concerned regime. The fluctuation expansion approach works in the regime where the scale takes the positive value, which is separated from the other part of the whole parameter space by the boundary of the dashed line. On the other hand, the approach presented in this paper is valid at any point of the parameter space.

with $G = \sqrt{2}g\alpha_s$ and $\Delta = \Delta_0 - g^2|\alpha_s|^2/\omega_m$ expressed in terms of the cavity field amplitude $\alpha_s = E/(\kappa + i\Delta)$ as the stationary solution to the Langevin equation. The workable regime for the fluctuation expansion approach is depicted with these conditions in Fig. 6. Both of the approaches work in the red detuned regime. Fig. 7, however, shows that even in this common regime the entanglement between the fluctuations can be very different from the OMS entanglement discussed in this paper.

As we mentioned at the beginning, the fluctuation expansion approach works with approximating the OMS operators with the sum of their mean values following classical dynamics without noise drives and the fluctuations evolving according to quantum mechanics. Then

in the study of Gaussian state entanglement for OMS. Starting from our initial OMS quantum state (the cavity in a vacuum state and the mechanical oscillator in a thermal state), such entanglement for the evolved quantum state develops as the optomechanical coupling in Fig. 1 starts with the cavity field being built up by an external drive $E(t)$. Meanwhile, the generated entanglement is also weakened or even destroyed by the noise drives. The entanglement in the same regime was well studied in the fluctuation expansion approach [11–19]. The steady entanglement of the cavity and mechanical fluctuation is based on the classical steady state of OMS, the existence of which is determined by Routh-Hurwitz criterion [50] in terms of the following inequalities [11]:

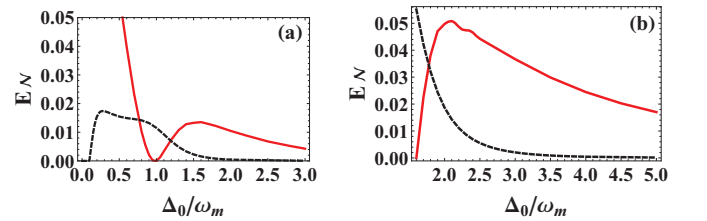


FIG. 7: Comparison of entanglement obtained in our approach (solid curve) and in the fluctuation expansion approach of [11] (dashed curve). (a) is obtained with the drive intensity $E/\kappa = 3 \times 10^5$ while (b) is for a drive of $E/\kappa = 2 \times 10^6$. The system parameters are $g/\kappa = 10^{-6}$, $\omega_m/\kappa = 2.5$, $\omega_m/\gamma_m = 10^7$, and $T = 0$. The entanglement represented by the solid curves is obtained at $\kappa t = 15$.

the system operators in the system-reservoir coupling of (2) are replaced by their fluctuations, so that only delta-function correlated Langevin noises $\hat{\xi}_c$ and $\hat{\xi}_m$ independent of cavity drive detuning and intensity are relevant to the linearized dynamics about the fluctuations and their entanglement. Instead, in our fully quantum approach, the linearized dynamics for the system operators in weak coupling regime involves the magnified noise drives due to the cubic term $-g(\hat{b} + \hat{b}^\dagger)\hat{a}^\dagger\hat{a}$ of the original OMS Hamiltonian; see Eq. (5). The difference of the quantum noise effects is expected to be experimentally tested by the measurement of cavity fluctuation amplitude. As illustrated in Fig. 8, the cavity fluctuations found in the different approaches drastically deviate with drive intensity. This phenomenon also indicates the distinct quantum states due to the different linearized dynamics. Our concerned OMS quantum states and those of the fluctuations around classical steady states can be seen to be

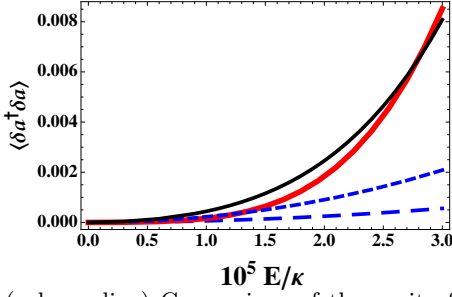


FIG. 8: (color online) Comparison of the cavity fluctuation $\langle \delta \hat{a}^\dagger \delta \hat{a} \rangle = \langle (\hat{a}^\dagger - \langle \hat{a}^\dagger \rangle)(\hat{a} - \langle \hat{a} \rangle) \rangle = \langle \hat{a}^\dagger \hat{a} \rangle - \langle \hat{a}^\dagger \rangle \langle \hat{a} \rangle$ at zero temperature obtained in the approach of the present work (solid curves) and in the fluctuation expansion approach of Ref. [11] (dashed curves). The plots for our approach are obtained at the time $\kappa t = 15$. The thick solid (red) and long dashed curves compare the fluctuation at the detuning $\Delta_0 = \omega_m$, while the thin solid (black) and short dashed compare that at $\Delta_0 = 0.5\omega_m$.

different from their CMs, which are in one-to-one correspondence to the respective Gaussian states. The entanglement for the evolved states of fully quantum OMS can thus significantly differ from that previously considered in the fluctuation expansion approach.

V. CONCLUSION

In conclusion, we have studied the dynamically generated entanglement of quantum OMSs that are initially in thermal equilibrium with their environment. The meaning of our research manifests in two aspects. First, one sees that high and robust entanglement for fully quantum OMSs can be generated with blue detuned drive. In

contrast, the previous fluctuation expansion approximation working under the classical steady state condition specifies an upper bound for the entanglement in blue detuned regime and only focuses on the steady entanglement under red detuned drives. This finding involving the different implementations is important to the related experimental studies on OMSs entering quantum regime. Second, our fully quantum dynamical approach shows that the noise effect on a quantum OMS drastically differs from that affecting the cavity and mechanical fluctuation considered in the previous approach, though the system dynamics is linearized for weak optomechanical coupling in both approaches. In the regime where the magnified noise effect is significant, complicated evolution patterns such as entanglement sudden death and revival exist for our concerned macroscopic entanglement. Such non-trivial quantum noise effect can also exist in other quantum nonlinear systems.

Acknowledgments

B.H. thanks M. Hillery for helpful conversations. This work was supported by AITF and NSERC. Q. L. acknowledges the support by NSFC(No. 11005040), NCETFJ(No. 2012FJ-NCET-ZR04), PPYMTSTRHU (No. ZQN-PY113) and CSC.

Appendix A: Factorization of Joint System-Reservoir Evolution Operator

Our discussion is based on the two following factorizations for a unitary evolution operator $U(t, 0) = \mathcal{T} \exp\{-i \int_0^t d\tau (H_1(\tau) + H_2(\tau))\}$ involving two processes described by $H_1(t)$ and $H_2(t)$, respectively:

$$\mathcal{T} e^{-i \int_0^t d\tau (H_1(\tau) + H_2(\tau))} = \mathcal{T} e^{-i \int_0^t d\tau H_1(\tau)} \mathcal{T} e^{-i \int_0^t d\tau V_1^\dagger(\tau, 0) H_2(\tau) V_1(\tau, 0)}, \quad (\text{A-1})$$

and

$$\mathcal{T} e^{-i \int_0^t d\tau (H_1(\tau) + H_2(\tau))} = \mathcal{T} e^{-i \int_0^t d\tau V_2(t, \tau) H_1(\tau) V_2^\dagger(t, \tau)} \mathcal{T} e^{-i \int_0^t d\tau H_2(\tau)}, \quad (\text{A-2})$$

where $V_k(t, \tau) = \mathcal{T} \exp\{-i \int_\tau^t d\tau' H_k(\tau')\}$ for $k = 1, 2$. The operator $U(t, 0)$ is the solution to the differential equations $dU/dt = -i(H_1(t) + H_2(t))\hat{U}(t)$, while $V_1(t, 0) = \mathcal{T} \exp\{-i \int_0^t d\tau H_1(\tau)\}$ is the solution to $dV_1/dt = -iH_1(t)V_1(t)$. The initial condition for the differential equations is $U(0, 0) = V_1(0, 0) = I$, the identity operator. The differential of $W(t, 0) = V_1^\dagger(t, 0)U(t, 0)$ with respect to t gives

$$\frac{dW}{dt} = -V_1^\dagger \frac{dV_1}{dt} V_1^\dagger U + V_1^\dagger \frac{dU}{dt} = iV_1^\dagger H_1 V_1 \hat{V}_1^\dagger \hat{U} - iV_1^\dagger (H_1 + H_2) \hat{U} = -iV_1^\dagger H_2 V_1 W. \quad (\text{A-3})$$

One has the solution to the above differential equation as $W(t, 0) = \mathcal{T} \exp\{-i \int_0^t d\tau V_1^\dagger(\tau, 0) H_2(\tau) V_1(\tau, 0)\}$, thus proving the factorization in (A-1). By exchanging $H_1(t)$ and $H_2(t)$ in (A-1), one has the factorization of the operator

$U(t, 0)$ as

$$V_2(t, 0) \mathcal{T} e^{-i \int_0^t d\tau V_2^\dagger(\tau, 0) H_1(\tau) V_2(\tau, 0)} = V_2(t, 0) \mathcal{T} e^{-i \int_0^t d\tau V_2^\dagger(\tau, 0) H_1(\tau) V_2(\tau, 0)} V_2^\dagger(t, 0) V_2(t, 0).$$

Because $V_2(t, 0)$ is a unitary operation, one can rewrite the right side of the above as $\mathcal{T} e^{-i \int_0^t d\tau V_2(t, \tau) H_1(\tau) V_2^\dagger(t, \tau)} V_2(t, 0)$, giving the form in Eq.(A-2). Here we have used the relation $V_2(t, 0) V_2^\dagger(\tau, 0) = V_2(t, \tau)$.

We first apply Eq. (A-2) to factorize $U_D(t, 0) = \mathcal{T} \exp\{-i \int_0^t d\tau H_D(\tau)\}$ out of the system-reservoir evolution operator $U_S(t, 0) = \mathcal{T} \exp\{-i \int_0^t d\tau (H_S(\tau) + H_D(\tau))\}$, where $H_S(\tau)$ and $H_D(\tau)$ are given in Eqs. (1) and (2) of the main text, respectively. In this way one has

$$U_S(t, 0) = \mathcal{T} \exp\{-i \int_0^t d\tau U_D(t, \tau) H_S(\tau) U_D^\dagger(t, \tau)\} \mathcal{T} \exp\{-i \int_0^t d\tau H_D(\tau)\}. \quad (\text{A-4})$$

The cavity mode operator \hat{a} in $H_S(\tau)$ is transformed to

$$U_D(t, \tau) \hat{a} U_D^\dagger(t, \tau) = e^{-\frac{\kappa}{2}(t-\tau)} \hat{a} + \hat{n}_c(t, \tau) \equiv \hat{A}(t, \tau) \quad (\text{A-5})$$

in $U_D(t, \tau) H_S(\tau) U_D^\dagger(t, \tau)$, and the mechanical mode operator is transformed to

$$U_D(t, \tau) \hat{b} U_D^\dagger(t, \tau) = e^{-\frac{\gamma_m}{2}(t-\tau)} \hat{b} + \hat{n}_m(t, \tau) \equiv \hat{B}(t, \tau), \quad (\text{A-6})$$

where $\hat{n}_c(t, \tau) = \sqrt{\kappa} \int_\tau^t d\tau' e^{-\kappa(\tau'-\tau)/2} \hat{\xi}_c(\tau')$ and $\hat{n}_m(t, \tau) = \sqrt{\gamma_m} \int_\tau^t d\tau' e^{-\gamma_m(\tau'-\tau)/2} \hat{\xi}_m(\tau')$ [29]. The transformed operators satisfy the equal-time commutation relation $[\hat{A}(t, \tau), \hat{A}^\dagger(t, \tau)] = [\hat{B}(t, \tau), \hat{B}^\dagger(t, \tau)] = 1$. Then the Hamiltonian in the first time-ordered exponential of (A-4) becomes

$$U_D(t, \tau) H_S(\tau) U_D^\dagger(t, \tau) = (iE(t) \hat{A}^\dagger(t, \tau) e^{i\Delta_0 t} - iE^*(t) \hat{A}(t, \tau) e^{-i\Delta_0 t}) - g \hat{K}_m(t, \tau) \hat{A}^\dagger \hat{A}(t, \tau), \quad (\text{A-7})$$

where

$$\hat{K}_m(t, \tau) = \cos(\omega_m \tau) (\hat{B}_m(t, \tau) + \hat{B}_m^\dagger(t, \tau)) + \sin(\omega_m \tau) (-i \hat{B}_m(t, \tau) + i \hat{B}_m^\dagger(t, \tau)).$$

By using (A-1) we factorize out the drive Hamiltonian in (A-7) as follows:

$$\begin{aligned} & \mathcal{T} \exp\{-i \int_0^t d\tau U_D(t, \tau) H_S(\tau) U_D^\dagger(t, \tau)\} \\ &= \mathcal{T} \exp\left\{-i \int_0^t d\tau (iE(t) \hat{A}^\dagger(t, \tau) e^{i\Delta_0 t} - iE^*(t) \hat{A}(t, \tau) e^{-i\Delta_0 t}) \mathcal{T} \exp\left\{ig \int_0^t d\tau U_E^\dagger(\tau, 0) \hat{K}_m(t, \tau) \hat{A}^\dagger \hat{A}(t, \tau) U_E(\tau, 0)\right\}\right\} \\ &= \mathcal{T} \exp\left\{-i \int_0^t d\tau (iE(t) \hat{A}^\dagger(t, \tau) e^{i\Delta_0 t} - iE^*(t) \hat{A}(t, \tau) e^{-i\Delta_0 t})\right\} \\ &\times \mathcal{T} \exp\left\{ig \int_0^t d\tau \hat{K}_m(t, \tau) (\hat{A}^\dagger(t, \tau) + D^*(\tau)) (\hat{A}(t, \tau) + D(\tau))\right\}, \end{aligned} \quad (\text{A-8})$$

where $U_E(\tau, 0) = \mathcal{T} \exp\{\int_0^\tau dt' E(t') e^{i\Delta_0 t'} \hat{A}^\dagger(t, t') - H.c.\}$. In (A-8) the effect of $U_E(\tau, 0)$ on the cavity operator $\hat{A}(t, \tau)$ is the displacement

$$\begin{aligned} U_E^\dagger(\tau, 0) \hat{A}(t, \tau) U_E(\tau, 0) &= \hat{A}(t, \tau) + e^{-\frac{\kappa}{2}(t-\tau)} \int_0^\tau dt' E(t') e^{i\Delta_0 t'} e^{-\frac{\kappa}{2}(t-t')} + \int_0^\tau dt' \Gamma_c(t', \tau) E(t') e^{i\Delta_0 t'} \\ &\equiv \hat{A}(t, \tau) + D(\tau), \end{aligned} \quad (\text{A-9})$$

where

$$\Gamma_c(t', \tau) = [\hat{n}_c(t, t'), \hat{n}_c^\dagger(t, \tau)] = e^{-\kappa(\tau-t')/2} - e^{-\kappa(t-\tau)/2} e^{-\kappa(t-t')/2}.$$

The next step is to factorize the second time-ordered exponential in (A-8) as follows:

$$\begin{aligned} & \mathcal{T} \exp\left\{ig \int_0^t d\tau \hat{K}_m(t, \tau) (\hat{A}^\dagger(t, \tau) + D^*(\tau)) (\hat{A}(t, \tau) + D(\tau))\right\} \\ &= \mathcal{T} \exp\left\{ig U_K(t, \tau) (\hat{K}_m(t, \tau) (\hat{A}^\dagger(t, \tau) D(\tau) + \hat{A}(t, \tau) D^*(\tau) + |D(\tau)|^2) U_K^\dagger(t, \tau))\right\} \\ &\times \mathcal{T} \exp\left\{ig \int_0^t d\tau \hat{K}_m(t, \tau) \hat{A}^\dagger \hat{A}(t, \tau)\right\}, \end{aligned} \quad (\text{A-10})$$

where $U_K(t, \tau) = \mathcal{T} \exp\{ig \int_{\tau}^t dt' \hat{K}_m(t, t') \hat{A}^{\dagger} \hat{A}(t, t')\}$. To the first order of g , the operation $U_K(t, \tau)$ in the first time-ordered exponential of the above equation transforms the mechanical operator as

$$U_K(t, \tau) \hat{K}_m(t, \tau) U_K^{\dagger}(t, \tau) = \hat{K}_m(t, \tau) - 2g \int_{\tau}^t dt' e^{-\gamma_m(\tau' - \tau)/2} \sin \omega_m(\tau - \tau') \hat{A}^{\dagger}(t, \tau') \hat{A}(t, \tau') + \dots \quad (\text{A-11})$$

and the cavity operator $\hat{A}(t, \tau)$ as

$$U_K(t, \tau) \hat{A}(t, \tau) U_K^{\dagger}(t, \tau) = \hat{A}(t, \tau) - ig \int_{\tau}^t dt' e^{-\kappa(t' - \tau)/2} \hat{K}_m(t, t') \hat{A}(t, t') + \dots \quad (\text{A-12})$$

The neglected higher order terms in the above expansions are successively lowered by a small factor in the order of $g(t - \tau)$, because all terms in the expansions only contain the operators \hat{K}_m and \hat{A} not magnified by the drive intensity $E(t)$, so the dominant first order contribution leads to the effective optomechanical coupling Hamiltonian

$$\tilde{H}_{OM}(\tau) = -g \hat{K}_m(t, \tau) (D^*(\tau) \hat{A}(t, \tau) + D(\tau) \hat{A}^{\dagger}(t, \tau) + |D(\tau)|^2) \quad (\text{A-13})$$

for the first time-ordered exponential in (A-10), which is defined as $U_{OM}(t, 0) = \mathcal{T} \exp\{-i \int_0^t d\tau \tilde{H}_{OM}(\tau)\}$. Now we have exactly factorized the joint evolution operator as

$$U_S(t, 0) = U_E(t, 0) U_{OM}(t, 0) U_K(t, 0) U_D(t, 0). \quad (\text{A-14})$$

Appendix B: Expectation Value of System Operators

We apply the factorization of the joint evolution operator in (A-14) to find the expectation value of a system operator \hat{O} :

$$\begin{aligned} \text{Tr}_S\{\hat{O}\rho(t)\} &= \text{Tr}_S\{\hat{O} \text{Tr}_R\{U_E(t, 0) U_{OM}(t, 0) U_K(t, 0) U_D(t, 0) \rho(0) R(0) U_D^{\dagger}(t, 0) U_K^{\dagger}(t, 0) U_{OM}^{\dagger}(t, 0) U_E^{\dagger}(t, 0)\}\} \\ &= \text{Tr}_{S \otimes R}\{U_{OM}^{\dagger}(t, 0) U_E^{\dagger}(t, 0) \hat{O} U_E(t, 0) U_{OM}(t, 0) (U_K(t, 0) U_D(t, 0) \rho(0) R(0) U_D^{\dagger}(t, 0) U_K^{\dagger}(t, 0))\}. \end{aligned} \quad (\text{B-1})$$

The action $U_K(t, 0) U_D(t, 0) \rho(0) R(0) U_D^{\dagger}(t, 0) U_K^{\dagger}(t, 0)$ is on the the product of the initial system state

$$\rho(0) = |0\rangle_c \langle 0| \otimes \sum_{n=0}^{\infty} \frac{n_m^n}{(1 + n_m)^{n+1}} |n\rangle_m \langle n| \equiv |0\rangle_c \langle 0| \otimes \rho_m \quad (\text{B-2})$$

and the associate reservoir state $R(0)$ in thermal equilibrium with $\rho(0)$, where n_m is the thermal phonon number at the temperature T .

We first look at $U_D(t, 0) \chi(0) U_D^{\dagger}(t, 0)$, where $\chi(0) = \rho(0) R(0)$ and

$$U_D(t, 0) = \mathcal{T} \exp \left\{ \int_0^t d\tau (\sqrt{\gamma_m} \hat{b}^{\dagger} \hat{\xi}_m(\tau) - \sqrt{\gamma_m} \hat{b} \hat{\xi}_m^{\dagger}(\tau)) \right\} \mathcal{T} \exp \left\{ \int_0^t d\tau (\sqrt{\kappa} \hat{a}^{\dagger} \hat{\xi}_c(\tau) - \sqrt{\kappa} \hat{a} \hat{\xi}_c^{\dagger}(\tau)) \right\}.$$

The second operator of the cavity and vacuum reservoir coupling does not change $\chi(0)$ because

$$(\sqrt{\kappa} \hat{a}^{\dagger} \hat{\xi}_c(\tau) - \sqrt{\kappa} \hat{a} \hat{\xi}_c^{\dagger}(\tau)) |0\rangle_C = 0 \quad (\text{B-3})$$

for the product state $|0\rangle_C$ of the cavity vacuum and its associate vacuum reservoir. If the action of the first operator involving mechanical mode and mechanical reservoir coupling changes the joint initial state $\chi(0)$, the system state

$$\tilde{\rho}(t) = \text{Tr}_R \left\{ \mathcal{T} e^{\int_0^t d\tau \{\sqrt{\gamma_m} \hat{b}^{\dagger} \hat{\xi}_m(\tau) - \sqrt{\gamma_m} \hat{b} \hat{\xi}_m^{\dagger}(\tau)\}} \chi(0) \mathcal{T} e^{-\int_0^t d\tau \{\sqrt{\gamma_m} \hat{b}^{\dagger} \hat{\xi}_m(\tau) - \sqrt{\gamma_m} \hat{b} \hat{\xi}_m^{\dagger}(\tau)\}} \right\}$$

evolved under such coupling will be different from $\rho(0)$. The system quantum state $\tilde{\rho}(t)$ is the solution to the master equation

$$\dot{\tilde{\rho}} = \gamma_m (n_{th} + 1) \{ \hat{b} \tilde{\rho}(t) \hat{b}^{\dagger} - \frac{1}{2} \tilde{\rho}(t) \hat{b}^{\dagger} \hat{b} - \frac{1}{2} \hat{b}^{\dagger} \tilde{\rho}(t) \} + \gamma_m n_{th} \{ \hat{b}^{\dagger} \tilde{\rho}(t) \hat{b} - \frac{1}{2} \tilde{\rho}(t) \hat{b} \hat{b}^{\dagger} - \frac{1}{2} \hat{b} \hat{b}^{\dagger} \tilde{\rho}(t) \} \quad (\text{B-4})$$

in Lindblad form [44]. The initial state for the above master equation is $\tilde{\rho}(0) = \rho_m$, and n_{th} is the thermal quantum number of the reservoir. Here we assume the possible non-equilibrium between system and reservoir, so that n_{th} could be different from n_m (in the main text we only consider the situation of thermal equilibrium). This master equation can be exactly solved by the super-operator technique [51] as

$$\tilde{\rho}(t) = \sum_{n=0}^{\infty} \frac{(n_{th} + (n_m - n_{th})e^{-\gamma_m t/2})^n}{(1 + n_{th} + (n_m - n_{th})e^{-\gamma_m t/2})^{n+1}} |n\rangle_m \langle n|. \quad (\text{B-5})$$

If the system and reservoir is in thermal equilibrium, i.e. $n_{th} = n_m$, the above state will be ρ_m constantly with time. Under this condition, therefore, the operation $U_D(t, 0)$ keeps the joint initial state $\chi(0)$ invariant. Moreover, similar to (B-3), one has $U_K(t, 0)\chi(0)U_K^\dagger(t, 0) = \chi(0)$. Thus the system operator expectation value in (B-1) will reduce to the form in (7) of the main text.

Appendix C: Calculation of Entanglement Measured by Logarithmic Negativity

The entanglement of bipartite Gaussian states is quantified via the correlation matrix

$$\hat{V} = \begin{pmatrix} \hat{A} & \hat{C} \\ \hat{C}^T & \hat{B} \end{pmatrix}. \quad (\text{C-1})$$

with the elements $\hat{V}_{ij}(t) = 0.5\langle \hat{u}_i \hat{u}_j + \hat{u}_j \hat{u}_i \rangle - \langle \hat{u}_i \rangle \langle \hat{u}_j \rangle$, where $\hat{u} = (\hat{x}_c(t), \hat{p}_c(t), \hat{x}_m(t), \hat{p}_m(t))^T$. The logarithmic negativity as a measure for the entanglement is given as [45, 52]

$$E_N = \max[0, -\ln 2\eta^-], \quad (\text{C-2})$$

where

$$\eta^- = \frac{1}{\sqrt{2}} \sqrt{\Sigma - \sqrt{\Sigma^2 - \det \hat{V}}} \quad (\text{C-3})$$

and

$$\Sigma = \det \hat{A} + \det \hat{B} - 2\det \hat{C}. \quad (\text{C-4})$$

$U_E(t, 0)$ in (B-1) does not contribute to the correlation matrix elements. Given the quadratic Hamiltonian H_{OM} in (6) of the main text, the operation U_{OM} transforms the vector $(\hat{x}_c(t), \hat{p}_c(t), \hat{x}_m(t), \hat{p}_m(t))^T$ in terms of the following linear differential equation:

$$\begin{aligned} \frac{d}{d\tau} \begin{pmatrix} \hat{x}_c \\ \hat{p}_c \\ \hat{x}_m \\ \hat{p}_m \end{pmatrix} &= \begin{pmatrix} 0 & 0 & l_3(t, \tau) & l_4(t, \tau) \\ 0 & 0 & l_1(t, \tau) & l_2(t, \tau) \\ -l_2(t, \tau) & l_4(t, \tau) & 0 & 0 \\ l_1(t, \tau) & -l_3(t, \tau) & 0 & 0 \end{pmatrix} \begin{pmatrix} \hat{x}_c \\ \hat{p}_c \\ \hat{x}_m \\ \hat{p}_m \end{pmatrix} + \begin{pmatrix} \hat{f}_1 \\ \hat{f}_2 \\ \hat{f}_3 \\ \hat{f}_4 \end{pmatrix} \\ &\equiv \frac{d}{d\tau} \hat{v} = \hat{M}(t, \tau) \hat{v} + \hat{f}(t, \tau), \end{aligned} \quad (\text{C-5})$$

where

$$\begin{aligned} l_1(t, \tau) &= g e^{-\kappa(t-\tau)/2 - \gamma_m(t-\tau)/2} (D(\tau) + D^*(\tau)) \cos(\omega_m \tau), \\ l_2(t, \tau) &= g e^{-\kappa(t-\tau)/2 - \gamma_m(t-\tau)/2} (D(\tau) + D^*(\tau)) \sin(\omega_m \tau), \\ l_3(t, \tau) &= i g e^{-\kappa(t-\tau)/2 - \gamma_m(t-\tau)/2} (D(\tau) - D^*(\tau)) \cos(\omega_m \tau), \\ l_4(t, \tau) &= i g e^{-\kappa(t-\tau)/2 - \gamma_m(t-\tau)/2} (D(\tau) - D^*(\tau)) \sin(\omega_m \tau), \end{aligned} \quad (\text{C-6})$$

and

$$\begin{aligned} \hat{f}_1(t, \tau) &= \frac{i}{\sqrt{2}} g e^{-\kappa(t-\tau)/2} (D(\tau) - D^*(\tau)) \{ \cos(\omega_m \tau) (\hat{n}_m(t, \tau) + \hat{n}_m^\dagger(t, \tau)) - \sin(\omega_m \tau) (i \hat{n}_m(t, \tau) - i \hat{n}_m^\dagger(t, \tau)) \}, \\ \hat{f}_2(t, \tau) &= \frac{1}{\sqrt{2}} g e^{-\kappa(t-\tau)/2} (D(\tau) + D^*(\tau)) \{ \cos(\omega_m \tau) (\hat{n}_m(t, \tau) + \hat{n}_m^\dagger(t, \tau)) - \sin(\omega_m \tau) (i \hat{n}_m(t, \tau) - i \hat{n}_m^\dagger(t, \tau)) \}, \\ \hat{f}_3(t, \tau) &= -g (\hat{n}_c(t, \tau) D^*(\tau) + \hat{n}_c^\dagger(t, \tau) D(\tau) + |D(\tau)|^2) e^{-\gamma_m(t-\tau)/2} \sin(\omega_m \tau), \\ \hat{f}_4(t, \tau) &= g (\hat{n}_c(t, \tau) D^*(\tau) + \hat{n}_c^\dagger(t, \tau) D(\tau) + |D(\tau)|^2) e^{-\gamma_m(t-\tau)/2} \cos(\omega_m \tau). \end{aligned} \quad (\text{C-7})$$

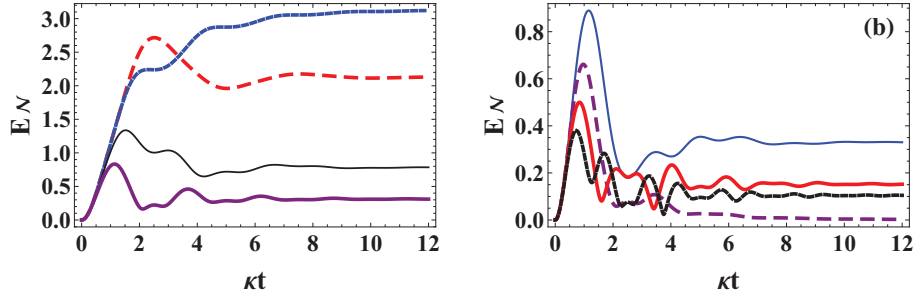


FIG. C-1: Entanglement evolution without quantum noise effect. (a) Blue detuned regime. The long dashed (red) curve is for $\Delta_0 = -0.5\omega_m$, the short dashed (blue) curve for $\Delta_0 = -\omega_m$, the thin solid (black) curve for $\Delta_0 = -1.5\omega_m$, and the thick solid (purple) curve for $\Delta_0 = -2\omega_m$. (b) Red detuned regime. The thin solid (blue) curve is for $\Delta_0 = 0.5\omega_m$, and the long dashed (purple) curve for $\Delta_0 = \omega_m$, the solid (red) curve for $\Delta_0 = 1.5\omega_m$, and the short dashed (black) curve for $\Delta_0 = 2\omega_m$. The system parameters are $g/\kappa = 10^{-6}$, $E/\kappa = 2 \times 10^6$, $\omega_m/\kappa = 2.5$, $\omega_m/\gamma_m = 10^7$, and $T = 0$. The plots in (a) and (b) correspond to those in Fig. 1(b) and Fig. 2(b) of the main text, respectively. Here the entanglement without the effect of quantum noises becomes steady with time, while that under quantum noise effect shown in the main text could be destroyed after a finite period of time.

In the above the terms containing \hat{n}_c , \hat{n}_m and their conjugates contribute to the correlation matrix (C-1), and the pure drive terms proportional to $|D(\tau)|^2$ do not contribute to \hat{V} , but they affect the system mean motion $\langle \hat{v}_i(t) \rangle$. The solution to (C-5) is

$$\hat{v}(t) = \mathcal{T} e^{\int_0^t d\tau \hat{M}(t,\tau)} \hat{v}(0) + \mathcal{T} e^{\int_0^t d\tau \hat{M}(t,\tau)} \int_0^t d\tau (\mathcal{T} e^{\int_0^\tau d\tau' \hat{M}(t,\tau')})^{-1} \hat{f}(t,\tau). \quad (\text{C-8})$$

In the general situation the time-ordered exponentials in the solution (C-8) should be expanded to infinite series (Magnus expansion [53]) for numerical calculations. Given a cavity drive with its profile $|E(t)| \leq C$ (C is a constant) such that the function $D(t)$ defined in (A-9) is bounded, the decay factor $e^{-(\kappa+\gamma_m)(t-\tau)/2}$ dominates the behavior of the matrix $\hat{M}(t,\tau)$, so one has the approximate commutator $[\hat{M}(t,\tau_1), \hat{M}(t,\tau_2)] \approx 0$ in the concerned regimes in which $gE(t)$ is not very large. Then the time-ordered exponentials in the above solution can be replaced by the ordinary exponentials to have a closed form of the solution to the differential equation (C-5) as

$$\begin{aligned} \hat{v}(t) &\approx e^{\int_0^t d\tau \hat{M}(t,\tau)} \hat{v}(0) + \int_0^t e^{\int_\tau^t d\tau' \hat{M}(t,\tau')} \hat{f}(t,\tau) d\tau \\ &= (\cosh(\sqrt{m(t,0)}) \hat{I} + \frac{\sinh(\sqrt{m(t,0)})}{\sqrt{m(t,0)}} \hat{K}(t,0)) \hat{v}(0) \\ &\quad + \int_0^t d\tau (\cosh(\sqrt{m(t,\tau)}) \hat{I} + \frac{\sinh(\sqrt{m(t,\tau)})}{\sqrt{m(t,\tau)}} \hat{K}(t,\tau)) \hat{f}(t,\tau). \end{aligned} \quad (\text{C-9})$$

Here we have defined $\hat{K}(t,\tau) = \int_\tau^t d\tau' \hat{M}(t,\tau')$, and the function $m(t,\tau)$ from the relation $\hat{K}^2(t,\tau) = m(t,\tau) \hat{I}$ is

$$m(t,\tau) = \frac{1}{4} \left| \int_\tau^t d\tau' (l_1(t,\tau') + il_2(t,\tau') - il_3(t,\tau') + l_4(t,\tau')) \right|^2 - \frac{1}{4} \left| \int_\tau^t d\tau' (l_1(t,\tau') - il_2(t,\tau') - il_3(t,\tau') - l_4(t,\tau')) \right|^2. \quad (\text{C-10})$$

With arbitrary system parameters, the first term in (C-8) from the initial value $\hat{v}(0)$ of system operators contributes to one part of the correlation matrix $\hat{V}_1(t)$, where the average in the calculation of the matrix elements is taken with respect to the initial system state $\rho(0)$. This reflects the reliance of the system quantum state at the time t on this initial state. Meanwhile, the second term of noise driving leads to another part of the correlation matrix $\hat{V}_2(t)$, where the average is over the reservoir state $R(0)$. Summing up the two matrices gives the total correlation matrix $\hat{V}(t) = \hat{V}_1(t) + \hat{V}_2(t)$. For a comparison with the entanglement evolution found in the main text, we give an example of entanglement evolution solely determined by matrix $\hat{V}_1(t)$ in Fig. (C-1). In the absence of quantum noise effect, the entanglement measured by logarithmic negativity tends to stable value with time, and there does not exist the phenomenon of entanglement sudden death in Fig. 1 and 2 of the main text.

-
- [1] G. J. Milburn and M. J. Woolley, *Acta Physica Slovaca* 61, 483 (2011).
- [2] Y. Chen, *J. Phys. B: At. Mol. Opt. Phys.* 46, 104001 (2013).
- [3] M. Aspelmeyer, T. J. Kippenberg, and F. Marquardt, arXiv:1303.0733.
- [4] A. H. Safavi-Naeini, *et al.*, *Phys. Rev. Lett.* 108, 033602 (2012).
- [5] N. Brahms, *et al.*, *Phys. Rev. Lett.* 108, 133601 (2012).
- [6] E. Verhagen, S. Deléglise, S. Weis, A. Schliesser, and T. J. Kippenberg, *Nature* 482, 63 (2012).
- [7] T. P. Purdy, R. W. Peterson, and C. A. Regal, *Science* 339, 801 (2013).
- [8] T. A. Palomaki, J. W. Harlow, J. D. Teufel, R. W. Simmonds, and K. W. Lehnert, *Nature* 495, 210 (2013).
- [9] T. P. Purdy, P.-L. Yu, R. W. Peterson, N. S. Kampel, and C. A. Regal, *Phys. Rev. X* 3, 031012 (2013).
- [10] M. Hillery, *Acta Physica Slovaca* 59, 1 (2009).
- [11] D. Vitali, *et al.*, *Phys. Rev. Lett.* 98, 030405 (2007).
- [12] M. Paternostro, *et al.*, *Phys. Rev. Lett.* 99, 250401 (2007).
- [13] D. Vitali, P. Tombesi, M. J. Woolley, A. C. Doherty, and G. J. Milburn, *Phys. Rev. A* 76, 042336 (2007).
- [14] C. Genes, A. Mari, P. Tombesi, and D. Vitali, *Phys. Rev. A* 78, 032316 (2008).
- [15] M. J. Hartmann and M. B. Plenio, *Phys. Rev. Lett.* 101, 200503 (2008).
- [16] F. Galve, L. A. Pachon, and D. Zueco, *Phys. Rev. Lett.* 105, 180501 (2010).
- [17] C.-L. Zou, X.-B. Zou, F.-W. Sun, Z.-F. Han, and G.-C. Guo, *Phys. Rev. A* 84, 032317 (2011).
- [18] M. Abdi, S. Barzanjeh, P. Tombesi, and D. Vitali, *Phys. Rev. A* 84, 032325 (2011).
- [19] R. Ghobadi, A. R. Bahrampour, and C. Simon, *Phys. Rev. A* 84, 033846 (2011).
- [20] A. Mari and J. Eisert, *Phys. Rev. Lett.* 103, 213603 (2009).
- [21] A. Mari and J. Eisert, *New J. Phys.* 14, 075014 (2012).
- [22] A. Farace and V. Giovannetti, *Phys. Rev. A* 86, 013820 (2012).
- [23] S. G. Hofer, W. Wieczorek, M. Aspelmeyer, and K. Hammerer, *Phys. Rev. A* 84, 052327 (2011).
- [24] G. Wang, L. Huang, Y.-C. Lai, and C. Grebogi, *Phys. Rev. Lett.* 112, 110406 (2014).
- [25] F. Marquardt, J. G. E. Harris, and S. M. Girvin, *Phys. Rev. Lett.* 96, 103901 (2006).
- [26] P. Rabl, *Phys. Rev. Lett.* 107, 063601 (2011).
- [27] A. Nunnenkamp, K. Børkje, and S. M. Girvin, *Phys. Rev. Lett.* 107, 063602 (2011).
- [28] J.-Q. Liao, H. K. Cheung, and C. K. Law, *Phys. Rev. A* 85, 025803 (2012).
- [29] B. He, *Phys. Rev. A* 85, 063820 (2012).
- [30] J.-Q. Liao and F. Nori, arXiv:1304.6612.
- [31] B. Pepper, R. Ghobadi, E. Jeffrey, C. Simon, and D. Bouwmeester, *Phys. Rev. Lett.* 109, 023601 (2012).
- [32] S. Basiri-Esfahani, U. Akram, and G. J. Milburn, *New J. Phys.* 14, 085017 (2012).
- [33] X.-W. Xu, Y.-J. Li, and Y.-x. Liu, *Phys. Rev. A* 87, 025803 (2013).
- [34] X.-W. Xu, H. Wang, J. Zhang, and Y.-x. Liu, *Phys. Rev. A* 88, 063819 (2013).
- [35] X.-X. Ren, H.-K. Li, M.-Y. Yan, Y.-C. Liu, Y.-F. Xiao, and Q. Gong, *Phys. Rev. A* 87, 033807 (2013).
- [36] U. Akram, W. P. Bowen, and G. J. Milburn, *New J. Phys.* 15, 093007 (2013).
- [37] K. Stannigel, *et al.*, *Phys. Rev. Lett.* 109, 013603 (2012).
- [38] M. Ludwig, A. H. Safavi-Naeini, O. Painter, and F. Marquardt, *Phys. Rev. Lett.* 109, 063601 (2012).
- [39] X.-Y. Lü, W.-M. Zhang, S. Ashhab, Y. Wu, and F. Nori, *Scientific Reports* 3, 2943 (2013).
- [40] J.-Q. Liao, K. Jacobs, F. Nori, and R. W. Simmonds, *New J. Phys.* 16, 072001 (2014).
- [41] M. Ludwig, B. Kubala, and F. Marquardt, *New J. Phys.* 10, 095013 (2008).
- [42] J. Qian, A. A. Clerk, K. Hammerer, and F. Marquardt, *Phys. Rev. Lett.* 109, 253601 (2012).
- [43] S. Kiesewetter, Q. Y. He, P. D. Drummond, and M. D. Reid, arXiv: 1312.6474.
- [44] C. W. Gardiner and P. Zoller, *Quantum Noise* (Springer-Verlag, Berlin, 2000).
- [45] G. Adesso, A. Serafini, and F. Illuminati, *Phys. Rev. A* 70, 022318 (2004).
- [46] T. Yu and J. H. Eberly, *Phys. Rev. Lett.* 93, 140404 (2004).
- [47] T. Yu and J. H. Eberly, *Science* 323, 598 (2009).
- [48] M. R. Vanner, *et al.*, *Proc. Natl. Acad. Sci. USA* 108, 16182 (2011).
- [49] M. R. Vanner, J. Hofer, G. D. Cole, and M. Aspelmeyer, *Nat. Comm.* 4, 2295 (2013).
- [50] I. S. Gradshteyn and I. M. Ryzhik, *Table of Integrals, Series and Products* (Academic Press, Orlando, 2000).
- [51] L. M. Arévalo-Aguilar and H. Moya-Cessa, *J. Opt. B: Quantum Semiclass. Opt.* 10, 671 (1998).
- [52] G. Vidal and R. F. Werner, *Phys. Rev. A* 65, 032314 (2002).
- [53] W. Magnus, *Commun. Pure Appl. Math.* 7, 649 (1954).